Chinese Chemical Letters 37 (2026) 112410

Contents lists available at ScienceDirect

Chinese Chemical Letters

journal homepage: www.elsevier.com/locate/cclet

Si–O doped layered carbon-based catalyst boosts nonradical oxidation pathways *via* peroxymonosulfate activation for refractory organic pollutants removal

Cheng Han[a], Lanlan Liang[a], Jiao Yang[a], Yin Wei[a], Zhe Zhang[a], Haonan Chen[a], Wei Yu[a], Chuanliang Zhao[a,*], Liwei Yang[a,*], Bo Lai[b]

[a] Key Laboratory of Water Supply & Sewage Engineering of Ministry of Housing and Urban-rural Development, School of Civil Engineering, Chang'an University, Xi'an 710061, China
[b] State Key Laboratory of Hydraulics and Mountain River Engineering, College of Architecture and Environment, Sichuan University, Chengdu 610065, China

ARTICLE INFO

Article history:
Received 20 August 2025
Revised 16 November 2025
Accepted 12 January 2026
Available online 13 January 2026

Keywords:
Carbon-based catalysts
Si–O doped
Peroxymonosulfate
Singlet oxygen
Density functional theory calculations

ABSTRACT

Traditional carbon-based catalysts often suffer from limited catalytic activity and stability in peroxymonosulfate (PMS) activation for pollutant degradation. In this study, a Si–O doped layered carbonaceous catalyst (Si/C@PDA) was synthesized using natural vermiculite as the hard template, enabling the efficient PMS activation for ultrafast degradation of tetracycline (TC) ($k_{obs\text{-}TC} = 0.228$ min^{-1}). The Si/C@PDA/PMS system demonstrated strong resistance to environmental matrix interference by enhanced singlet oxygen ($^1O_2$) generation and electron transfer processes (ETP). The experimental and density functional theory results prove that the Si–O site induced the cleavage of adsorbed PMS to promote the generation of $^1O_2$ through the self-decomposition of peroxymonosulfate anion radical ($SO_5^{\bullet-}$) and the disproportionation of superoxide radical ($O_2^{\bullet-}$). Meanwhile, the Si–O site also served as the electron transfer bridge facilitating electron migration from the pollutants to the Si/C@PDA/PMS*. In addition, the Si/C@PDA/PMS system integrated with membrane filtration technology achieved continuous degradation of TC with nearly 100% removal efficiency under a low oxidant dosage (0.1 mmol/L PMS). This work underscores the pivotal role of Si–O doping in modulating active sites to selectively promote nonradical pathways, thereby promoting effective pollutant degradation in complex water matrices and offering strategic insights for developing nonradical-dominated carbon-based catalysts.

© 2026 Published by Elsevier B.V. on behalf of Chinese Chemical Society and Institute of Materia Medica, Chinese Academy of Medical Sciences.

Recently, the widespread occurrence of refractory organic pollutants in the environment has posed significant risks to aquatic ecosystems and human health [1]. It is essential to develop efficient technologies for the removal of refractory organic pollutants. Among various treatment technologies, peroxymonosulfate-based advanced oxidation processes (PMS-AOPs) have gained considerable attention due to the advantages of strong oxidation capacity, high stability, and wide application [2–5]. Recent studies have shown that PMS-AOPs exhibit multiple pollutant degradation pathways, which can be generally divided into radical and nonradical pathways [6,7]. For radical pathways, various reactive oxygen species (ROS) with strong oxidation capacity such as hydroxyl radicals ($^{\bullet}OH$), sulfate radicals ($SO_4^{\bullet-}$), are *in situ* generated through the cleavage of the O–O bond in peroxymonosulfate (PMS) [8].

However, the radical pathway is highly sensitive to common constituents in real wastewater, such as inorganic anions (*e.g.*, Cl^-, HCO_3^-, NO_3^-) and organic matter (*e.g.*, humic acid (HA)). These substances can quench ROS (*e.g.*, $SO_4^{\bullet-}$, $^{\bullet}OH$), significantly reducing the pollutant degradation efficiency [3,9]. Nonradical pathways, including singlet oxygen ($^1O_2$) and electron transfer processes (ETP), have been extensively investigated as promising alternatives for achieving efficient and selective pollutant removal under complex water conditions. This is attributed to their longer lifetimes, resistance to radical scavengers, and reduced interference from background constituents in actual wastewater [4,5,10,11].

Carbon-based catalysts have emerged as promising materials for PMS activation *via* nonradical pathways. This is due to their tunable surface properties, chemical stability, and tendency to mediate a nonradical pathway [8,10,12]. Nevertheless, the widespread adoption of carbon-based catalysts is still constrained by their moderate catalytic activity and stability [11,13]. Recent studies have demonstrated that heteroatom doping, defect engineering,

* Corresponding authors.
E-mail addresses: zhaochuanliang90@sina.com (C. Zhao), yanglw61@163.com (L. Yang).

https://doi.org/10.1016/j.cclet.2026.112410
1001-8417/© 2026 Published by Elsevier B.V. on behalf of Chinese Chemical Society and Institute of Materia Medica, Chinese Academy of Medical Sciences.

and graphitized structure can significantly enhance the catalytic activity of carbon-based catalysts [10,12,14,15]. In particular, doping with heteroatoms of varying electronegativity (*e.g.*, N, P, O, Si) can modulate the electronic structure to adjust surface charge distribution. This facilitates the adsorption of PMS on active sites and promotes the generation of nonradicals [10,14–16]. Among these, Si–O bonds have shown great potential in facilitating PMS activation due to the large electronegativity difference between Si (1.90) and O (3.44) [10]. However, their specific role and underlying mechanism in boosting PMS activation for the generation of nonradicals remain unclear [14,17].

Vermiculite (VMT), a natural silicate mineral, possesses a unique layered structure, excellent adsorption capacity, and notable cation exchange properties [18,19]. Owing to these physicochemical characteristics, VMT can serve as a source of Si and O for incorporation into carbon-based catalysts, modulating their surface electronic structure and thereby enhancing PMS activation. Furthermore, VMT serves as a hard template to promote the formation of porous layered frameworks, enhancing the contact between PMS and active sites and thereby accelerating the catalytic reactions. These advantages make VMT a promising candidate for fabricating Si–O doped layered carbon-based catalysts for PMS activation, providing new insights into the Si–O-mediated mechanism for inducing nonradical pathways.

In this study, a novel Si–O-doped porous layered carbon catalyst (Si/C@PDA) was synthesized using VMT as both a structural template and Si–O source *via* the polymerization of dopamine under alkaline conditions followed by calcination and acid etching (Texts S1 and S2 in Supporting information). The structural and compositional properties of Si/C@PDA were thoroughly characterized. Its catalytic performance and degradation mechanisms were investigated using multiple techniques, including quenching tests, electron paramagnetic resonance (EPR), electrochemical measurements, and density functional theory (DFT) simulations (Texts S3–S13, Table S1 in Supporting information).

The scanning electron microscope (SEM) showed that the VMT has a layered structure (Fig. 1a) and the thickness of layer was uneven (Fig. 1b). The Si/C@PDA successfully retained the layered structure of the VMT template (Fig. 1c). The transmission electron microscope (TEM) images further confirmed that the precursor (Si/C@PDA pre) and Si/C@PDA exhibited a layered structure (Fig. 1d and Fig. S1 in Supporting information). The primary elements in VMT were Al, Si, and O, while Si/C@PDA pre mainly consisted of C and Al (Fig. 1b and Fig. S1c). In contrast, Si/C@PDA was primarily composed of C, N, O, and Si (Fig. 1d). The above results indicated that a Si–O doped layered carbon-based catalyst was successfully synthesized using VMT as a hard template.

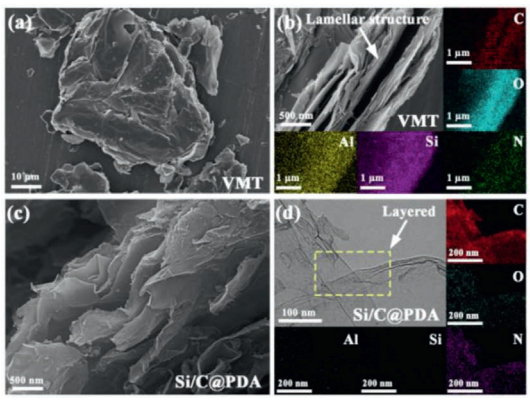


Fig. 1. (a) SEM and (b) energy dispersive X-ray spectroscopy (EDS) element mapping images of VMT. (c) SEM, (d) TEM and EDS element mapping images of Si/C@PDA.

The chemical states of catalysts were probed by X-ray photoelectron spectroscopy (XPS). As presented in Fig. S2a (Supporting information), the XPS survey spectra indicated the existence of C, Si, and O in Si/C@PDA. In the XPS Si 2p spectra of Si/C@PDA, a distinct peak corresponding to Si–O–C appeared at 101.82 eV, and the Si–O peak was observed at 103.36 eV (Fig. 2a and Table S2 in Supporting information) [10,17]. Compared with VMT (102.65 eV), the Si–O peak in Si/C@PDA showed a significant red shift of 0.71 eV. This shift indicated an altered electronic environment around the Si atoms, likely resulting from covalent bonding between Si–O and the carbon matrix [20]. The XPS spectra of C 1s revealed significant differences in carbon content and composition between VMT and Si/C@PDA (Fig. 2b and Table S2). Si/C@PDA exhibited a markedly higher proportion of C–C bonds compared to other carbon bond types. The XPS N 1s spectra of Si/C@PDA revealed the presence of graphitic N, pyridinic N and pyrrolic N (Fig. 2c and Table S2) [21].

X-ray diffraction (XRD) was used to investigate the differences in the crystal structure of the catalyst (Fig. 2d and Fig. S2b in Supporting information). The XRD patterns indicated that VMT was primarily composed of quartz (PDF #79–1905). Si/C@PDA showed characteristic patterns of graphitic carbon and SiO_2 (PDF #65–466), indicating a composition dominated by carbon-based materials and quartz. The Raman spectrum results indicated that the I_D/I_G ratio of Si/C@PDA was 1.50, which was higher than that of C@PDA, suggesting that Si/C@PDA had a higher degree of defects (Fig. 2e). N_2 adsorption-desorption analysis revealed a mesoporous structure in Si/C@PDA. This was further confirmed by the pore size distribution (Fig. 2f and Fig. S2c in Supporting information). Furthermore, Si/C@PDA exhibited a specific surface area of 70.6 m^2/g, which was substantially higher than that of pristine VMT (6.4 m^2/g) (Table S3 in Supporting information).

As illustrated in Fig. S3 (Supporting information), the negligible oxidation observed with PMS alone indicated its ineffectiveness in degrading tetracycline (TC). Meanwhile, Si/C@PDA alone achieved approximately 30 % TC removal, primarily attributed to adsorption. The Si/C@PDA/PMS system achieved over 95 % removal of TC, exhibiting an apparent reaction rate constant (k_{obs}) of 0.228 min^{-1}. This value is 22.8 times higher than that of PMS alone (Fig. S4a in Supporting information). This enhanced activity could be attributed to the synergistic interaction between Si–O bonds and the carbon matrix, promoting electron transfer and ROS generation. A comparative analysis of the oxidation capabilities of various carbon-based and metal-based catalysts for pollutant degradation is presented in Fig. S5 and Table S4 (Supporting information). Among these, the Si/C@PDA/PMS system demonstrated exceptional catalytic performance, surpassing most carbon-based catalysts and even exceeding that of many metal-based systems.

The effects of catalyst dosages, PMS concentration, and initial pH on pollutant degradation were investigated (Fig. 3 and Fig. S4 in Supporting information). Considering both catalytic efficiency and cost-effectiveness, the optimal conditions for subsequent experiments were determined to be the catalyst dosage of 0.1 g/L and the PMS concentration of 0.5 mmol/L. The effect of solution pH in Si/C@PDA/PMS system is presented in Fig. 3a. Across the pH range of 3.0–7.0, the Si/C@PDA/PMS system exhibited robust catalytic performance with 100 % TC removal. Meanwhile, the TC removal decreased from 100 % to 92 % as the pH increased from 7.0 to 11.0, which could be attributed to the enhanced self-decomposition of PMS under alkaline conditions [22]. The results indicated that the Si/C@PDA/PMS/TC system exhibited a broad pH applicability range. To assess potential interferences in actual wastewater, the effects of representative inorganic anions and organic matter on TC removal were systematically investigated. The Si/C@PDA/PMS system achieved the removal efficiency of over 97 % for TC with the addition of 10 mmol/L anions (Fig. 3b). With the increase in HA concentration from 10 mg/L to 30 mg/L, the Si/C@PDA/PMS system main-

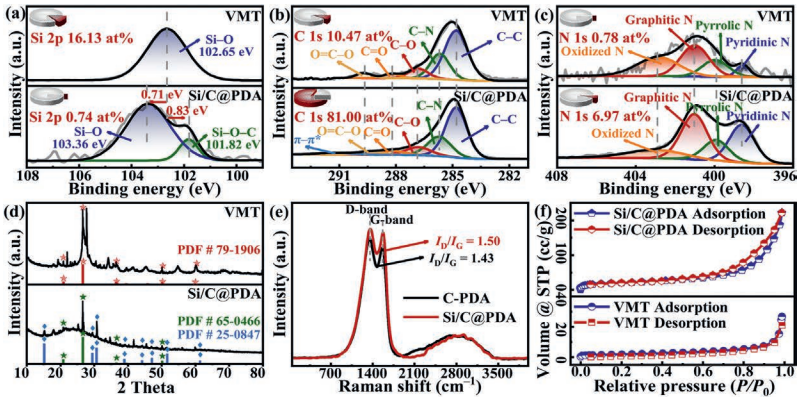


Fig. 2. (a) XPS Si 2p, (b) XPS C 1s, (c) XPS N 1s, and (d) XRD patterns of VMT and Si/C@PDA. (e) Raman spectra and (f) N_2 adsorption-desorption isotherms.

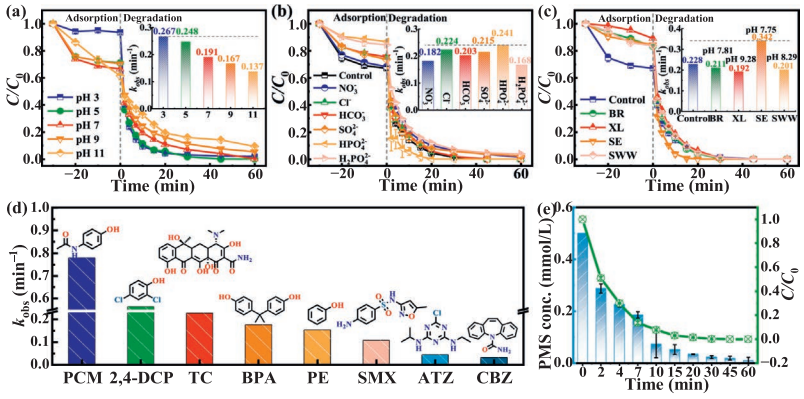


Fig. 3. Effects of (a) different pH values, (b) coexisting anions in water, and (c) actual water on TC removal. (d) Removal of various pollutants, and (e) PMS residual concentration in the Si/C@PDA/PMS system. Ba river water (BR, from the Ba river in Xi'an), Xiuyuan lake water (XL, from Xi'an), groundwater (SWW, from Weinan), and secondary effluent (SE, from a municipal wastewater treatment plant in Xi'an). Reaction conditions: [catalyst] = 0.1 g/L, [pH]$_0$ 7, [PMS]$_0$ = 0.5 mmol/L, [organics] = 10 mg/L, [anions] = 10 mmol/L, T = 25 °C. The error bars represent the standard deviation (n = 3).

tained the TC removal efficiency of over 94 % (Fig. S6 in Supporting information). The degradation performance of the Si/C@PDA/PMS system in real water matrices was further evaluated (Fig. 3c and Fig. S7, Table S5 in Supporting information). Four types of real water samples were used in the experiments. Fig. 3c showed that the Si/C@PDA/PMS system achieved 100 % TC removal in all tested real water matrices, demonstrating excellent practical applicability. To evaluate the catalytic activity of Si/C@PDA toward various organic pollutants, different pollutants found in natural water were selected (Fig. 3d). The Si/C@PDA/PMS system achieved 100 % removal efficiency for paracetamol (PCM), 2,4-dichlorophenol (2,4-DCP), TC, and bisphenol A (BPA), with k_{obs} of 0.779, 0.564, 0.228, and 0.176 min^{-1}, respectively. Overall, the synthesized catalyst exhibited excellent degradation efficiency for various pollutants in complex water matrices.

Furthermore, the residual PMS concentration in the Si/C@PDA/PMS system was quantified *via* the 2,2′-azino-bis(3-ethylbenzothiazoline-6-sulfonic acid) diammonium salt (ABTS) method [23]. The remaining PMS concentration exhibited a degradation trend consistent with pollutant removal. Only 0.01 mmol/L PMS remained after 60 min, confirming that 98 % of the PMS was effectively activated for organic pollutant degradation (Fig. 3e).

The typical quenching tests and EPR measurements were carried out to directly verify ROS across various systems. EPR spectroscopy with 2,2,6,6-tetramethylpiperidine (TEMP) and 5,5-dimethyl-1-pyrroline *N*-oxide (DMPO) as spin-trapping agents was employed to identify and confirm the generation of ROS. DMPO was utilized to trap $^{\bullet}OH$ and $SO_4^{\bullet-}$, and TEMP was employed to capture $^1O_2$ [2–4]. As shown in Fig. 4a, the typical four-fold peaks with an intensity ratio of 1:2:2:1 were attributed to the DMPO-$^{\bullet}OH$ adduct in Si/C@PDA/PMS system. The characteristic sextet peaks of $SO_4^{\bullet-}$ were also observed in the Si/C@PDA/PMS system. Meanwhile, a strong signal of $^1O_2$ was detected, confirming the generation of $^1O_2$ in the Si/C@PDA/PMS system. *Tert*–butyl alcohol (TBA), methanol (MeOH), furfuryl alcohol (FFA) and TEMP were used as scavengers for $^{\bullet}OH$, $^{\bullet}OH/SO_4^{\bullet-}$, $^{\bullet}OH/^1O_2$, and $^1O_2$, respectively [10,24,25]. The addition of MeOH and TBA had minimal impact on TC degradation, indicating that $^{\bullet}OH$ and $SO_4^{\bullet-}$ played a relatively minor role in degradation process. In contrast, the specific $^1O_2$ quencher of FFA and TEMP exhibited a significant inhibitory effect on TC degradation, and this inhibition became more pronounced with increasing concentrations of the quencher. The results emphasized the critical role of $^1O_2$ in the degradation of pollutants (Figs. 4b and e). To further confirm the role of $^1O_2$ in the degradation process, deuterium oxide (D_2O) was used to replace pure water in the reaction system. The lifetime of $^1O_2$ in D_2O (~67.0 μs) is significantly longer than in pure water (~3.5 μs), which could theoretically enhance the degradation rate of pollutants [24,26]. This substitution promoted the k_{obs} of TC from 0.2314 min^{-1} to 0.3378 min^{-1}, reaffirming the role of $^1O_2$ in TC degradation (Fig. 4c).

Determining the source of oxygen for $^1O_2$ production is the first critical step in elucidating the mechanism of $^1O_2$ production. Two possible sources of oxygen in the Si/C@PDA/PMS system were explored, including dissolved oxygen and PMS [26]. The introduction of nitrogen or oxygen gas did not affect TC degradation, indicating that $^1O_2$ was not generated from dissolved oxygen (Fig. S8a in Supporting information) [27]. Typically, the generation of $^1O_2$

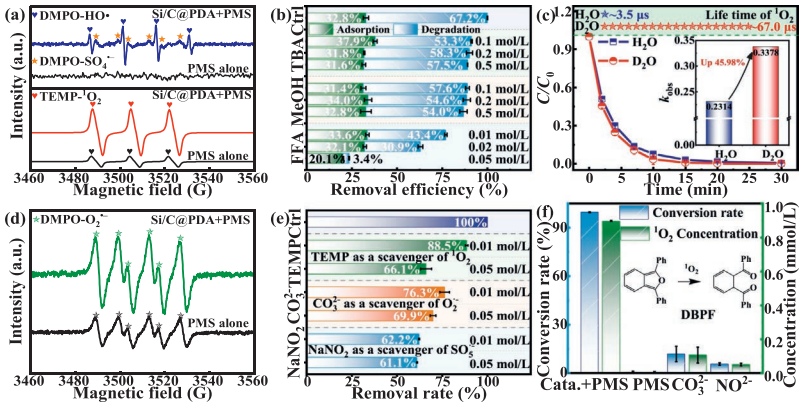


Fig. 4. (a) EPR spectra of the Si/C@PDA/PMS system. (b) Effects of various radical inhibitors on TC degradation. (c) Comparison of degradation efficiency of TC in H_2O and D_2O. (d) EPR spectra of DMPO. (e) Inhibitory effects of various scavengers on TC degradation. (f) Conversion rate of $^1O_2$. Reaction conditions: [catalyst] = 0.1 g/L, $[pH]_0$ 7, $[PMS]_0$ = 0.5 mmol/L, [organics] = 10 mg/L, T = 25 °C. The error bars represent the standard deviation (n = 3).

from PMS can be summarized into three pathways: (i) The surface carbonyl/ketone groups act as catalytic sites to activate PMS *via* nucleophilic addition to generate $^1O_2$ [28,29], (ii) the superoxide radical ($O_2^{\bullet-}$) mediated generation of $^1O_2$ through recombination or proton-promoted disproportionation [30], and (iii) the self-reaction of peroxymonosulfate anion radical ($SO_5^{\bullet-}$) generated $^1O_2$ ($PMS \rightarrow SO_5^{\bullet-} \rightarrow {}^1O_2$) [31]. To elucidate the mechanism of $^1O_2$ production, we investigated the possible PMS reaction pathways through refined experiments. First, no detectable changes in carbonyl or ketone (C=O) functional groups on the Si/C@PDA catalyst surface were observed before and after the reaction *via* Fourier transform infrared spectroscopy (FT-IR) analysis (Fig. S8b in Supporting information), thereby excluding the effect of surface carbonyl/ketone groups [26]. Second, the role of $^1O_2$ in TC removal was further confirmed by employing CO_3^{2-} and $NaNO_2$ as scavengers for $O_2^{\bullet-}$ and $SO_5^{\bullet-}$, respectively (Fig. 4e). The addition of CO_3^{2-} in the Si/C@PDA/PMS system inhibited the TC degradation, indicating that $^1O_2$ generation *via* the dismutation of $O_2^{\bullet-}$ occurred in the system. Meanwhile, EPR analysis confirmed the substantial generation of $O_2^{\bullet-}$ in the Si/C@PDA/PMS system (Fig. 4d). Upon the addition of $NaNO_2$, the TC removal efficiency of the Si/C@PDA/PMS system decreased to approximately 61 %, confirming that $^1O_2$ generation was also attributed to the self-decomposition of $SO_5^{\bullet-}$ facilitated by the catalyst (Fig. 4e).

To further quantify the generation of $^1O_2$, the fluorescent probe method was employed. 1,3-Diphenylisobenzofuran (DPBF), a well-established fluorescent probe for $^1O_2$, specifically reacted with $^1O_2$ to form an endoperoxide, which subsequently decomposed into 1,2-dibenzoylbenzene [23]. Since the molar ratio of DPBF degradation to $^1O_2$ consumption was 1:1, the $^1O_2$ concentration in the Si/C@PDA/PMS system was quantified based on the consumption of DPBF [23]. As shown in Fig. 4f, the Si/C@PDA/PMS system achieved 99.69 % DPBF conversion (0.897 mmol/L $^1O_2$), while the PMS-alone system showed only 0.58 % conversion (0.005 mmol/L $^1O_2$). Additionally, the addition of CO_3^{2-} and $NaNO_2$ as quenching agents in the Si/C@PDA/PMS/DBPF system further validated the $^1O_2$ generation pathway. Upon introducing these quenchers, the DPBF conversion rate decreased to 11.87 % and 5.56 %, with the corresponding $^1O_2$ concentrations reduced to 0.107 and 0.050 mmol/L, respectively. This indicated that $O_2^{\bullet-}$ and $SO_5^{\bullet-}$ served as intermediates in the decomposition of PMS for $^1O_2$ generation. These findings confirmed that $^1O_2$ in the Si/C@PDA/PMS system was generated through PMS decomposition *via* two distinct pathways: the dismutation of $O_2^{\bullet-}$ ($PMS \rightarrow O_2^{\bullet-} \rightarrow {}^1O_2$) and the self-decomposition of $SO_5^{\bullet-}$ ($SO_5^{\bullet-} \rightarrow S_2O_8^{\bullet-} + {}^1O_2$, or $SO_5^{\bullet-} \rightarrow SO_4^{\bullet-} + {}^1O_2$).

Quenching experiments did not completely suppress TC removal, suggesting additional degradation pathways. Therefore, possible ETP in the Si/C@PDA/PMS system was investigated using premixing experiments (Fig. S8c in Supporting information). The premixture of PMS and Si/C@PDA would exert negligible effects on TC removal, if the oxidation mechanism were primarily governed by ETP. Meanwhile, if both ETP and ROS were generated from Si/C@PDA/PMS system, extended premixture would reduce TC removal [32]. The TC removal efficiency decreased from 100 % to 61.8 % after 60 min of pre-mixing. The incomplete suppression of TC degradation suggested that in addition to $^1O_2$-mediated catalytic degradation, ETP also coexisted in the Si/C@PDA/PMS system.

Based on *in-situ* Raman analysis, the emergence of the characteristic peak at 832 cm^{-1} in the Si/C@PDA/PMS system confirmed the successful generation of PMS* [4,33], while the attenuation of this peak during TC degradation demonstrated the consumption of PMS* as the reactive species (Fig. S9 in Supporting information). Considering that electron transfer could occur from TC to Si/C@PDA/PMS* through an electron channel [10,34], the salt bridge experiment was conducted to further evaluate the ETP between TC and Si/C@PDA/PMS*. As illustrated in Fig. 5a, the Si/C@PDA achieved the highest peak current of 51.2 μA, followed sequentially by Si/C@PDA pre (35.9 μA), C@PDA (17.72 μA), blank (control, 14.9 μA), and VMT (8.1 μA). The salt bridge experiments demonstrated that the doped Si–O within Si/C@PDA facilitated ETP by enabling electron transfer from the TC to Si/C@PDA/PMS*. To further explore the ETP mechanism in the Si/C@PDA/PMS system, amperometric *i-t* curves were obtained under different PMS and TC addition sequences (Fig. 5b). At the initial stage, no electron transfer occurred between TC and Si/C@PDA. However, the addition of PMS significantly reduced the current density, confirming the occurrence of electron transfer between TC and Si/C@PDA/PMS* [35]. The ETP in the Si/C@PDA/PMS system was investigated through open-circuit potential (OCP) measurements. If a metastable complex does exist, then it would enhance the oxidation potential of Si/C@PDA [36]. As shown in Fig. 5c, the OCP change of Si/C@PDA was 0.31 eV (from 0.35 to 0.66 eV), while the changes for C@PDA, VMT, and the control were only 0.02, 0.13, and 0.23 eV, respectively. The results of the OCP analysis indicated that the formation of the metastable Si/C@PDA/PMS* accelerated the potential rise of Si/C@PDA [10,27,37]. Meanwhile, various pollutants were introduced into the electrochemical Si/C@PDA/PMS system, revealing two distinct potential decline patterns (Fig. 5d). Electron-deficient pollutants exhibited negligible decreases in potential, such as benzoic acid (BA, 0.0005 eV) and ibuprofen (IBU,

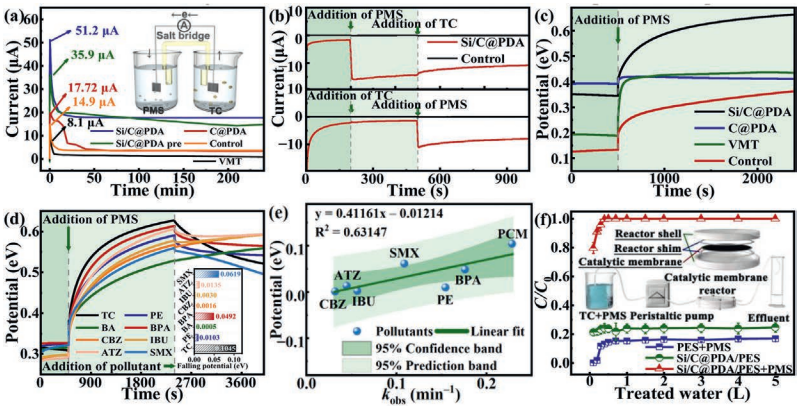


Fig. 5. (a) Relative current of salt bridge experiments. (b) Amperometric *i-t* curve measurements with sequential addition of PMS and TC. OCP of (c) catalyst electrode by adding PMS, and (d) Si/C@PDA electrode by adding PMS and pollutants. (e) Relationship between k_{obs} and potential decline. (f) TC removal of catalytic membrane reactor (TC = 500 μg/L, PMS = 0.1 mmol/L, Catalyst = 20 mg/L, Volume = 5 L). The error bars represent the standard deviation ($n = 3$).

0.0030 eV). In contrast, electron-rich pollutants, including BPA (0.0492 eV) and phenol (PE, 0.0103 eV), showed more pronounced potential reductions. Notably, TC demonstrated the highest potential drop (0.1045 eV) in the electrochemical Si/C@PDA/PMS system. The decline in OCP upon pollutant addition was ascribed to redox interactions between pollutants and Si/C@PDA/PMS*, resulting in the decomposition of surface complex [38]. Additionally, a linear relationship was observed between the k_{obs} of different pollutants removal and their corresponding potential (Fig. 5e, $R^2 = 0.631$). This correlation suggests that pollutants with lower half-wave potential tended to degrade faster in the Si/C@PDA/PMS system, a phenomenon consistent with reported ETP systems [39]. This result suggested that an ETP-based degradation pathway was also present in the Si/C@PDA/PMS system. To elucidate the dominant reactive species in the Si/C@PDA/PMS system, competitive kinetic experiments were performed using probe compounds (nitrobenzene, benzoic acid, and FFA) [27]. Results revealed that $^1O_2$ and ETP contributed 26.2 % and 68.3 %, respectively, while other ROS accounted for merely 5.5 % (Fig. S10 in Supporting information). These results demonstrate that TC degradation predominantly occurs through non-radical pathways in Si/C@PDA/PMS system.

The Si/C@PDA catalyst maintained a stable degradation efficiency of approximately 75 % after five cycles. Although the decline in activity could be attributed to active site blockage, its performance was effectively restored to over 95 % TC removal following a simple thermal regeneration process, highlighting the practical regenerability of the material (Fig. S11 in Supporting information) [11,13]. The Si/C@PDA membrane was constructed with polyethersulfone (PES) commercial membranes to investigate its potential for continuous water treatment (Fig. S12 in Supporting information). The contact angle measurement of the Si/C@PDA/PES membrane indicated that the catalytic membrane was hydrophilic (65.55°, Fig. S13 in Supporting information). The experimental procedure for continuous water treatment is illustrated in Fig. 5f and Fig. S14 (Supporting information). This facilitated mass transfer between pollutants and the catalytic membrane, which could contribute to pollutants degradation. Fig. 5f showed a comparison of the performance of the pure commercial PES membrane and Si/C@PDA/PES membrane to degrade TC. The Si/C@PDA/PES membrane system achieved continuous 100 % degradation of TC in 5 L solution with only 100 mg of Si/C@PDA under a low oxidant dosage (0.1 mmol/L PMS). In comparison, the Si/C@PDA system achieved only about 25 % removal of TC. The removal efficiency of pollutants by the catalytic membrane was further evaluated in various real water matrices. The results demonstrated that the Si/C@PDA/PMS system consistently maintained approximately 90 % TC removal rate (Fig. S15 in Supporting information). The membrane flux of the Si/C@PDA/PES membrane was 141.94 L h^{-1} m^{-2} (Fig. S16 in Supporting information). In summary, the results of continuous flow indicated that the Si/C@PDA/PES membrane showed considerable potential for practical use in wastewater treatment.

DFT analysis was conducted to validate the mechanistic role of Si–O in generating $^1O_2$ and ETP during PMS activation. The optimized structures are shown in Fig. S17 (Supporting information). The computational results indicated that the adsorption energies of PMS on C@PDA, N/C@PDA, and Si/C@PDA were –0.30, –0.55, and –0.69 eV, respectively (Fig. 6a). The strong adsorption induced by Si–O doping ensures intimate contact between PMS and active sites, creating favorable conditions for electron transfer and bond cleavage [10,16,17]. Additionally, the DFT results demonstrated that Si–O doping regulated the electronic configuration at the catalyst surface, breaking the uniformity of surface electron density and thereby promoting PMS adsorption and activation (Figs. 6b-e) [24,40].

As presented in Table S6 (Supporting information), the bond length of S–O_3 was longer than other bonds in the adsorbed PMS molecule. Additionally, the O–H bond length in the PMS molecule within the Si/C@PDA/PMS system (0.984 Å) was greater than that in free PMS (0.962 Å). This elongation weakens the O–H bond, thereby facilitating its cleavage and the subsequent formation of $SO_5^{\bullet-}$, which confirms the PMS-derived $^1O_2$ generation pathway [24,41]. Additionally, Si–O doping collectively impacted the dynamics of charge transfer at the interface. As is illustrated in Figs. 6f-i, the electric density difference results confirmed efficient electron transfer mediated by Si–O bridges between Si/C@PDA and PMS. The charge transfer characteristics of the relevant adsorption structures were further evaluated. Si/C@PDA (0.2835 e^-) demonstrated superior electron transfer compared to both N/C@PDA (0.2354 e^-) and C@PDA (0.1619 e^-). This enhancement was attributed to the Si–O doping, which facilitated faster electron mobility. The resulting efficient electron shuttling from the catalyst to the adsorbed PMS molecule is crucial for promoting the cleavage of the O–O bond, thereby enabling more efficient PMS activation [27].

Furthermore, the ETP oxidation in the catalyst/PMS system was analyzed based on molecular orbital analysis. The prerequisite for ETP oxidation in the catalyst/PMS system was initiated by electron transfer from the highest occupied molecular orbital (HOMO) of the pollutant to the lowest unoccupied molecular orbital (LUMO) of catalyst/PMS [10,42]. The gap between $LUMO_{(Si/C@PDA/PMS)}$ and $HOMO_{(TC)}$ was smaller than that between $LUMO_{(C@PDA/PMS)}$ and $HOMO_{(TC)}$ (Fig. 6j). Additionally, the ETP oxidation of differ-

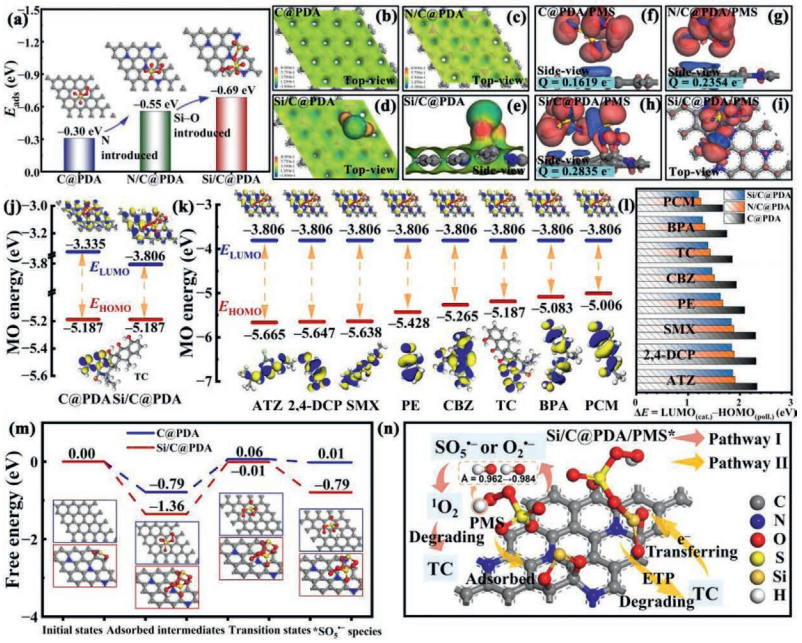


Fig. 6. (a) Adsorption energy of PMS on different structural models. (b) C@PDA, (c) N/C@PDA, (d, e) Si/C@PDA for electrostatic potential distributions. (f) C@PDA, (g) N/C@PDA, (h, i) Si/C@PDA for electric density difference. (j) The gap of $LUMO_{(catalysts)}$-$HOMO_{(TC)}$. (k) The $LUMO_{(Si/C@PDA/PMS)}$-$HOMO_{(pollutants)}$. (l) Different energy gaps between $LUMO_{(catalysts)}$ and $HOMO_{(pollutants)}$. (m) Free energy diagram and (n) schematic representation for PMS activation.

ent pollutants in the catalyst/PMS system was also calculated. As shown in Fig. 6k, varying energy gaps were observed between the $LUMO_{(Si/C@PDA/PMS)}$ and the $HOMO_{(pollutants)}$. The smaller gap between the $LUMO_{(Si/C@PDA/PMS)}$ and the $HOMO_{(pollutants)}$ indicated easier electron transfer from pollutants to Si/C@PDA/PMS by the Si–O bridge, thereby accelerating the ETP oxidation process (Fig. S18 in Supporting information). Moreover, the energy differences between the $LUMO_{(catalysts)}$ and the $HOMO_{(pollutants)}$ were compared. Notably, the Si/C@PDA/PMS system exhibited significantly smaller energy gaps with various pollutants compared to C@PDA/PMS and N/C@PDA/PMS system, further substantiating the promotion effects of Si–O doped in ETP oxidation (Fig. 6l and Table S7 in Supporting information).

As observed in Fig. 6m, the changes in reaction free energy for the Si/C@PDA/PMS system and C@PDA/PMS system were further calculated. Initially, PMS molecules were adsorbed onto the Si–O sites. Subsequently, the adsorbed PMS was activated, leading to the stretching and breaking of the O–H and Si–O bonds. Notably, the change of Si/C@PDA/PMS system in Gibbs free energy (ΔG) was negative, indicating that the reaction was spontaneous [24]. The released total energy during the reaction in the Si/C@PDA/PMS system was 0.79 eV, higher than that in the C@PDA/PMS system (0.01 eV), indicating that the Si/C@PDA/PMS system was both thermodynamically and kinetically advantageous for highly efficient pollutant degradation.

In summary, two distinct degradation mechanisms of TC in the Si/C@PDA/PMS system were verified (Fig. 6n). (i) PMS self-decomposed to produce $^1O_2$ through the self-decomposition of $SO_5^{\bullet-}$ and the disproportionation of $O_2^{\bullet-}$; (ii) PMS was adsorbed on Si/C@PDA to form Si/C@PDA/PMS*, which mediated electron transfer *via* the ETP pathway to drive TC oxidation.

The condensed Fukui index highlighted the reactive sites where active species in the Si/C@PDA/PMS system attacked TC. The spatial distributions of HOMO and LUMO of TC identified the regions prone to electron detachment and acceptance, with blue areas representing electron-rich regions and yellow areas representing electron-poor regions [43]. Fig. S19 (Supporting information) showed that f^-, f^+, and f^0 corresponded to the Fukui indices for susceptibility to electrophilic reagents, nucleophilic reagents, and radical, respectively. The high Fukui indices of O_{22} ($f^- = 0.161$), O_{23} ($f^- = 0.151$), O_{24} ($f^- = 0.058$), N_{21} ($f^- = 0.042$) suggested their vulnerability to electrophilic reagents like $^1O_2$ [22,43]. Besides, C_{10} ($f^+ = 0.096$), O_{22} ($f^+ = 0.086$), C_{11} ($f^+ = 0.08$), O_{26} ($f^+ = 0.074$), O_{25} ($f^+ = 0.07$) were prone to attack by nucleophilic reagents [22,43]. In addition, the high f^0 values of C_{10} and O_{23} were vulnerable to $SO_4^{\bullet-}$, $O_2^{\bullet-}$, $^{\bullet}OH$ attack.

Ultra-high-performance liquid chromatography-mass spectrometry (UHPLC-MS) analysis identified intermediate products in the Si/C@PDA/PMS/TC system, revealing 13 degradation intermediates (Fig. S20 and Table S8 in Supporting information). Based on the literature and DFT calculations, three possible degradation pathways for TC were proposed (Fig. 7a). In pathway I, TC was initially oxidized by $^1O_2$, forming the ketone compound **P1** (*m/z* 477). Subsequent oxidation by $^1O_2$ led to the formation of **P2** (*m/z* 361), accompanied by the loss of amide, methyl, and hydroxyl groups. Further oxidation and decomposition resulted in the formation of **P3** (*m/z* 274) [44,45]. In pathway II, $SO_4^{\bullet-}$ initially attacked the phenolic group of TC, leading to the formation of **P4** (*m/z* 432), which was subsequently oxidized and decomposed to **P5** (*m/z* 340). As degradation continued, ROS induced further oxidation and decomposition, leading to the formation of **P6** (*m/z* 238) [44,46]. In pathway III, TC underwent hydroxylation to yield **P7** (*m/z* 453), followed by demethylation of active species to form **P8** (*m/z* 417). This reaction was likely facilitated by the high electrophilic Fukui indices of O_{22} ($f^- = 0.161$) and O_{23} ($f^- = 0.151$) [47]. Additionally, two isomers (**P9** and **P10**) with *m/z* 340 were generated *via* dehydration condensation of hydroxyl groups at different positions [43]. These polycyclic intermediates were then oxidized into monocyclic or linear compounds (**P11**-**P14**), ultimately undergoing complete mineralization to produce CO_2 and H_2O.

Acute and chronic toxicity assessments of TC and its degradation products were performed using Toxicity Estimation Software Tool (TEST) and Ecological Structure Activity Relationships (ECOSAR) (Text S12 in Supporting information) [22,48]. The level

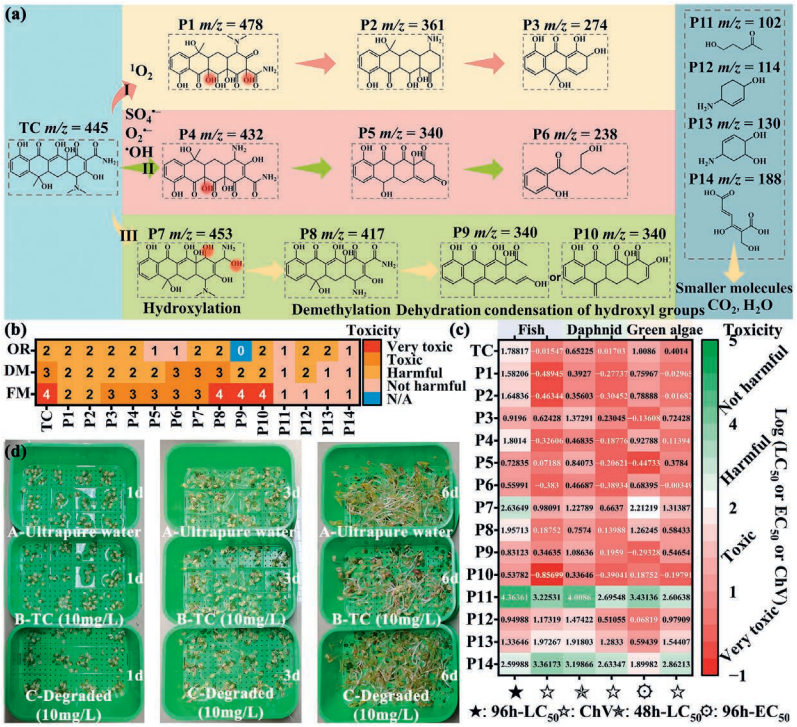


Fig. 7. (a) Proposed degradation pathways of TC. (b, c) Predicted toxicity of TC and its by-products in Si/C@PDA *via* TEST and ECOSAR. (d) Biological toxicity test of mung bean sprouts *via* ultrapure water, TC solution (10 mg/L) and degraded solution of TC.

of toxicity was evaluated by the rules of the Globally Harmonized System of Classification and Labelling of Chemicals (GHS). Heat maps from TEST and ECOSAR indicated that the acute and chronic toxicity of most degradation intermediates were lower than that of the original TC (Figs. 7b and c). However, some intermediates showed higher acute or chronic toxicity than TC toward certain species. For instance, intermediate **P8** exhibited increased acute toxicity to fathead minnow (FM), while **P10** demonstrated elevated chronic toxicity to fish, daphnid, and green algae. The mung bean sprout experiment (Fig. 7d) revealed that the TC solution significantly inhibited sprout development, with root length limited to only 2.65–2.80 cm during days 3–6, far shorter than the 8.92–9.84 cm observed in the degraded solution group. The degraded TC solution exhibited reduced toxicity, achieving shoot growth of 12.27 cm by day 6, comparable to the 12.56 cm in the pure water control (Figs. S21 and S22, Table S9 in Supporting information). Additionally, the germination rate in the degraded solution reached 98 %, compared to 93 % in the TC group, suggesting a relatively low toxicity of the TC solution after degradation [49]. The toxicity assessment showed that Si/C@PDA effectively activated PMS for the removal of TC, while promoting a more environmentally friendly degradation process.

In this work, a novel Si–O doped layered porous carbon-based catalyst was successfully synthesized using VMT as both a structural template and Si source. The catalyst exhibited exceptional PMS activation performance, achieving complete TC degradation ($k_{obs\text{-}TC} = 0.228$ min^{-1}) primarily through efficient nonradical pathways: $^1O_2$ and electron transfer. Both experimental results and DFT calculations confirmed that Si–O doping significantly modulated the surface electronic environment, facilitating strong electron interactions between Si/C@PDA and PMS. Furthermore, Si–O bonds played a crucial role in promoting O–H bond cleavage in PMS, leading to the formation of reactive intermediates ($SO_5^{\bullet-}$, $O_2^{\bullet-}$) and subsequent $^1O_2$ production. Practical evaluation using a Si/C@PDA catalytic membrane further demonstrated its applicability, achieving nearly 100 % TC degradation under a low PMS dosage (0.1 mmol/L). Compared to traditional carbon-based catalysts, the Si–O doping strategy employed here not only enhances PMS adsorption and electron transfer efficiency but also facilitates the selective cleavage of the O–H bond in PMS. These findings provide new insights into the role of Si–O doping in PMS activation and highlight the potential of carbon-based catalysts for efficient nonradical degradation of refractory organic pollutants in complex water environments.

CRediT authorship contribution statement

Cheng Han: Writing – original draft, Methodology, Formal analysis. **Lanlan Liang:** Writing – review & editing, Funding acquisition. **Jiao Yang:** Writing – review & editing, Methodology. **Yin Wei:** Writing – review & editing. **Zhe Zhang:** Writing – review & editing. **Haonan Chen:** Writing – review & editing, Investigation. **Wei Yu:** Methodology. **Chuanliang Zhao:** Writing – review & editing, Methodology, Funding acquisition. **Liwei Yang:** Writing – review & editing, Project administration, Funding acquisition. **Bo Lai:** Writing – review & editing, Supervision.

Declaration of competing interest

The authors declare that they have no known competing financial interests or personal relationships that could have appeared to influence the work reported in this paper.

Acknowledgments

Financial support for this research was provided by the Natural Science Basic Research Program of Shaanxi Province (Nos. 2024JC-YBMS-126 and 2024JC-YBMS-375) and the China Postdoctoral Science Foundation (No. GZC20250844).

Supplementary materials

Supplementary material associated with this article can be found, in the online version, at doi:10.1016/j.cclet.2026.112410.

References

[1] P. Chen, J. Wang, Y. Xue, et al., Water Res. 265 (2024) 122297.
[2] Y. Wang, D. Li, X. Ge, et al., Adv. Mater. 36 (2024) 2402935.
[3] C. Zhang, L. Chen, H. Luo, et al., Appl. Catal. B: Environ. 362 (2025) 124695.
[4] J. Xu, Y. Yao, C. Zhu, et al., Appl. Catal. B: Environ. 341 (2024) 123356.
[5] H. Li, X. Zhang, S. Yang, et al., Environ. Sci. Technol. 58 (2024) 14005–14012.
[6] N. Morin-Crini, E. Lichtfouse, M. Fourmentin, et al., Environ. Chem. Lett. 20 (2022) 1333–1375.
[7] Q. You, C. Zhang, M. Cao, et al., Appl. Catal. B: Environ. 338 (2023) 123025.
[8] N. Li, R. Li, X. Duan, et al., Environ. Sci. Technol. 55 (2021) 16163–16174.
[9] L. Zhai, F. Li, Y. He, et al., Chem. Eng. J. 478 (2023) 147378.
[10] J. Mao, K. Yin, Y. Zhang, et al., Appl. Catal. B: Environ. 342 (2024) 123428.
[11] X. Qiu, Y. Zhao, C. Li, et al., Chem. Eng. J. 483 (2024) 149265.
[12] X. Guo, Q. Zhang, H. He, et al., Appl. Catal. B: Environ. 335 (2023) 122886.
[13] S. Wang, J. Wang, Chem. Eng. J. 456 (2023) 141086.
[14] K. Yin, J. Yang, Y. Li, et al., Chin. Chem. Lett. 35 (2024) 109847.
[15] S. Xu, P. Wang, X. Mi, et al., J. Hazard. Mater. 466 (2024) 133321.
[16] J. Wang, Y. Qin, L. Li, et al., Chem. Eng. J. 457 (2023) 141253.
[17] T. Zhao, C. Tian, H. Li, et al., Chem. Eng. J. 491 (2024) 151878.
[18] C. Wang, B.H. Zhao, B.Y. Zhang, et al., J. Clean. Prod. 467 (2024) 142692.
[19] M. Tian, Y. Liu, S. Zhang, et al., Nat. Commun. 15 (2024) 391.
[20] A.S. Konashuk, E.O. Filatova, Phys. Chem. Chem. Phys. 19 (2017) 26201–26209.
[21] W. Kong, L. Huang, X. Quan, et al., Appl. Catal. B: Environ. 307 (2022) 121214.
[22] H. Chen, Y. Wei, C. Han, et al., Sep. Purif. Technol. 355 (2025) 129658.
[23] J. Song, N. Hou, X. Liu, et al., Adv. Mater. 36 (2024) 202405832.
[24] C.H. Gu, S. Wang, A.Y. Zhang, et al., Nat. Commun. 15 (2024) 5771.
[25] N. Chen, J. Xia, L. Li, et al., Surf. Interfaces 56 (2025) 105566.
[26] J. Zhen, J. Sun, X. Xu, et al., Angew. Chem. Int. Ed. 63 (2024) e202402669.
[27] C. Zhong, J. Wang, Y. Liu, et al., Appl. Catal. B: Environ. 370 (2025) 125193.
[28] S. Liu, Z. Zhang, F. Huang, et al., Appl. Catal. B: Environ. 286 (2021) 119921.
[29] H. Wang, C. Qiao, C. Chen, et al., Chin. Chem. Lett. 36 (2025) 110244.
[30] S. Jin, W. Shao, X. Luo, et al., Adv. Mater. 34 (2022) e2206516.
[31] L.S. Zhang, X.H. Jiang, Z.A. Zhong, et al., Angew. Chem. Int. Ed. 60 (2021) 21751–21755.
[32] R. Luo, M. Li, C. Wang, et al., Water Res. 148 (2019) 416–424.
[33] X. Zhao, J. Tong, S. Bai, et al., Appl. Catal. B: Environ. 379 (2025) 125654.
[34] M. Luo, H. Zhang, P. Zhou, et al., Water Res. 215 (2022) 118243.
[35] K. Yin, R. Wu, Y. Shang, et al., Appl. Catal. B: Environ. 329 (2023) 122558.
[36] Y. Wu, H. Wang, J. Du, et al., Environ. Sci. Technol. 57 (2023) 16662–16672.
[37] S. Liu, J. Du, H. Wang, et al., Water Res. 254 (2024) 121417.
[38] K. Yin, Y. Shang, D. Chen, et al., Appl. Catal. B: Environ. 338 (2023) 123029.
[39] P. Zhang, M. Sun, C. Zhou, et al., Environ. Sci. Technol. 58 (2024) 4781–4791.
[40] N.T. Dung, V.D. Thao, N.P. Thao, et al., Chem. Eng. J. 483 (2024) 149099.
[41] Z. Wu, Z. Xiong, B. Huang, et al., Nat. Commun. 15 (2024) 7775.
[42] C. Cheng, M. Xiong, L. Ding, et al., Appl. Catal. B: Environ. 344 (2024) 123616.
[43] Y. Liu, S. Liu, M. Chen, et al., J. Hazard. Mater. 461 (2024) 132417.
[44] X. Li, S. Wang, B. Xu, et al., Chem. Eng. J. 441 (2022) 136074.
[45] H. Huang, T. Guo, K. Wang, et al., Sci. Total. Environ. 758 (2021) 143957.
[46] X. Zhang, F. Wang, C. Wang, et al., Chem. Eng. J. 426 (2021) 131927.
[47] G. Kumar, R.K. Dutta, Process Saf. Environ. Protect. 159 (2022) 862–873.
[48] T. Liu, N. Li, S. Xiao, et al., Water Res. 265 (2024) 122270.
[49] M. Kang, X. Bai, Y. Liu, et al., Environ. Sci. Technol. 58 (2024) 9875–9886.